Himalayan Physics

Height profile variations of ionospheric conductivity: A case study in Addis Ababa, Ethiopia

https://doi.org/10.3126/hp.v11i1.57669

Lake Endeshaw[1]*

1 Department of Physics, Werabe University, Ethiopia

Abstract: Ionospheric conductivity is the ability to conduct ionospheric current and is impacted by a variety of current system flows in height profiles, which increase ionosphere conductivity. In this study, we have analyzed the height profiles of the ionospheric conductivity daily and monthly variations in Addis Ababa, Ethiopia, during a very low solar activity phase in the year 2020. The daily height profile variations of ionospheric conductivity in Addis Ababa with geographic latitude 9° N and longitude 39° E are estimated at midnight (00:00 UT), morning (09:00 UT), mid-day (12:00 UT), and early nighttime (18:00 UT). The monthly variations of ionospheric conductivity (parallel, Pedersen, and Hall conductivity) are also presented for all months, with the highest ionospheric variability occurring after noon (14.00 UT). At midnight (00:00 UT) and early nighttime (18:00 UT), the ionospheric conductivity shows more fluctuation than in the morning (09:00 UT) and midday (12:00 UT) in diurnal variation. The monthly variations of ionospheric conductivity (parallel, Pedersen, and Hall conductivity) in the daytime at 14:00 UT increase steeply to reach their peak values and keep the sharpness of their variability.

Keywords: Ionospheric variability • Parallel conductivity • Pedersen conductivity • Hall conductivity • Low solar activity

Recieved: 2024-03-04 **Revised: 2024-04-23** **Published: 2024-06-06**

I. Introduction

The upper region of the atmosphere, which is made up of a mixture of charged and neutral gases between approximately 50 and 2,000 km above the Earth's surface, is the ionosphere. The ionosphere has the advantage of absorbing the harmful radiation from the sun for all radio communication, navigation, and surveillance transmissions through it. Understanding the Earth's ionosphere entails deciphering the numerous changes in neutral and plasma density and their relationships to the coupling with the Earth's lower atmosphere, as well as the generation and flow of currents in the magnetosphere region. To further comprehend these problems, we have examined the composition and behavior of neutral and charged particles and field-aligned current, which describes the coupling of the ionosphere with the magnetosphere.

* *Corresponding Author: endeshawlake@gmail.com*

The description of this process affects the ionosphere and thermosphere regions to enhance coupling with the regions below and above at smaller spatial and temporal scales due to field-aligned plasma flow and ionospheric conductivity configuration [1–4].

In the ionosphere, at altitudes of about 80 to 500 km, there is a flow of several current systems [5]. This is a perpendicular current, and the field-aligned currents flow parallel to the Earth's magnetic field lines to connect the magnetospheric currents with polar ionospheric currents. The ring current plays a role in magnetosphere-ionosphere coupling; it flows at sunset in the equatorial magnetosphere, connecting the ionosphere with field-aligned currents and closing in on the ionosphere via the ionospheric current system. Most ionospheric current systems are governed by solar wind pressure and interplanetary magnetic fields (IMF), which cause geomagnetic activity to vary. Most magnetic perturbations are produced by ionospheric currents, and the electrons are magnetized and strongly bound to the Earth's magnetic field [6, 7].

Ionospheric conductivity is an important variable that is determined by the mobility of charged particles. It is affected by plasma, neutral density, charged particle gyro-frequencies, and collision frequencies. In the lower ionosphere, the conductivity provides the propagation of extremely low frequencies (0.003–3 kHz) [8]. The plasma is produced during the day by solar EUV radiation in the E-region; the conductivity is perpendicular to the magnetic field; and the F-region plays an important role in ionospheric conductivity with plasma transport [9–14]. Ionospheric plasma is generated by energetic ultraviolet solar radiation and particle precipitation at high latitudes. The current flow path is perpendicular to the magnetic field to indicate electromagnetic, gravitational, and plasma pressure gradient forces that are applied to the plasma density. This flow of current is the result of the spatial distribution of the source current and the ionospheric conductivity [15, 16]. Ionospheric conductivity moves the electrons across the geomagnetic field and drive an effective dynamo, providing the electromotive force, and the effective ionospheric conductivity is balanced between ion formation and recombination [17–20].

The ionosphere is a region of maximum plasma density, and it is where reflection, adsorption, and electric current take place. The ionospheric currents make a variation of the geomagnetic field in the earth's core. The ratio of gyro-frequencies to collision frequencies with height profiles determines ionospheric conductivity. The current flow is based on Ohm's law, and the geomagnetic field makes the electric conductivity anisotropic to present the parallel, Pedersen, and Hall conductivity [21–23]. The parallel conductivity is directed in parallel with the magnetic field, and it is greater than the other two ionospheric conductivities. The Pedersen conductivity is directed vertically with the magnetic field and parallelly with the electric field, whereas the Hall conductivity is directed vertically with both the magnetic and electric fields, and this is due to the drift motion of the electrons.

Several studies have shown that ionospheric current conductivity exists; some of them [24–29] have studied the existence of ionospheric currents, which is now experimentally confirmed by sounding satel-

lites. Moen and Brekke [30] and Robision et al. [31] investigated the indirect measurement of ionospheric conductivity from radar measurements of ionospheric electron density. Mcgranaghan et al. [32, 33] and Rasmussen et al. [34] investigated particle precipitation at the topside of the ionosphere using satellite measurements. Robinson and Vondrak [35] determined theoretically the relationship between the ionospheric conductivity and the major source of solar radiation. Richmond [36] studied this observation and concluded that both solar radiation and geomagnetic activity can affect the ionospheric conductivity. Friis-Christensen [17] defined the sources and relationship of ionospheric conductivity with solar magnetic field variation to the regular diurnal variation of the geomagnetic field. Richmond and Maute [37] have discussed different techniques of ionospheric wind dynamo modelling in a given neutral wind, ionospheric conductivity, and geomagnetic field. Ebihara et al. [38] have studied the possible influence of Hall conductivity on the resonant Alfven oscillations of the magnetosphere through the ionosphere reflection of the Alfven wave coefficient. Yue et al. [39] studied the influence of ionosphere conductivity on the ring current and found that storm-time ring current is significantly influenced by the interplanetary magnetic field (IMF), solar wind, solar radiation, and auroral activities. Shen et al. [40] and Qian and Solomon [41] initiated a data quality investigation for electron density at high latitudes and demonstrated the feasibility of utilizing the electron density profiles from COSMIC measurements, respectively, to estimate the ionospheric conductivity. Emmert [42] and Prolss [43] provided in-depth reviews of the large-scale neutral density variations. Liu et al. [44] described that the solar wind drives the neutral density variation.

In the study of ionospheric conductivity, influence, and variability, different researchers used different methods. Fuller-Rowell and Evans [45] determined global values of the Hall and Pedersen conductance for different levels of the Auroral Electrojet (AE) index. They used electron precipitation data from the Atmospheric Explorer (AE)-C and AE-D satellites. Kirkwood et al. [46] used the TIROS-NOAA satellite data to study the patterns of the height-integrated Pedersen and Hall conductivity. Aksnes et al. [47] used the European Incoherent Scatter (EISCAT) radar to examine the conductivity changes during sub-storms. They selected seven sub-storm events and measured the electron density profile in order to calculate the conductance. The Hall and Pedersen conductance reached 120 and 48 S/m, respectively. Giannattasio et al. [48] studied the instantaneous ionospheric global conductance maps during the sub-storm event occurring on July 31, 1997, by using the Polar Ionospheric X-ray Imager (PIXIE) and the Ultraviolet Imager (UVI) on board the Polar satellite data. At the start of the sub-storm expansion, the strongest conductance is observed in the per midnight sector. They observed that the Hall-to Pedersen conductance ratio in the regions of maximum Hall conductance increased throughout the event, indicating that the electron spectrum is hardening. Yue et al. [39] had used the International Reference Ionosphere (IRI-95) and Mass Spectrometer Incoherent Scatter (MSISE-90) to study the influence of the ionospheric conductivity on the ring current and calculate the background conductance. McGranagham et al. [33] provided the ionospheric Hall and Pedersen conductance variability as empirical orthogonal functions

(EOFs) from Defense Meteorological Satellite Program (DMSP) particle data. Singer et al. [23] studied the dependence of Pedersen conductance in the E and F regions and their ratio on the solar and geomagnetic activities by using the electron density profiles (EDPs) from the Constellation Observing System for Meteorology, Ionosphere, and Climate (COSMIC) data. Maeda [49] investigated parallel conductivity using in situ measurements of electron density and temperatures on the topside of the ionosphere and concluded that the asymmetry of conductivity from day to night is apparent and expected.

This study used the ionospheric conductivity model (height profile) of the World Data Center for Geomagnetism, Kyoto, to understand the height profiles of the parallel, Pedersen, and Hall conductivity and their variability of monthly and daily profiles over the Ethiopian ionosphere with very low solar activity. This may be the first work to extensively assess the three types of ionospheric conductivity during very low solar activity. As a result, this study considered the diurnal and monthly variability and the comparison of the three ionospheric conductivities in their height profiles.

II. Data and Methodology

The ionospheric conductivity acts on the Earth's upper atmosphere, which contains the maximum plasma density. This maximum free plasma density makes the variation of the geomagnetic field and the dynamo action generate the geomagnetic field in the Earth's centre. There are three types of ionospheric conductivity: parallel, Pedersen, and Hall conductivity. The ionospheric conductivity is measured by the SI unit Siemens per meter. The parallel conductivity is parallel to the magnetic field line; the Pedersen conductivity is in a vertical direction with a magnetic field and parallel with an electric field; and the Hall conductivity is also in a vertical direction with both electric and magnetic fields. In this study, we have analyzed the ionospheric conductivity model (height profile) of the World Data Center for Geomagnetism, Kyoto, to understand the height profiles of the parallel, Pedersen, and Hall conductivity and their variability of monthly and daily profiles over the Ethiopian ionosphere in a very low solar activity. The equations of ionospheric conductivity for the parallel (σ_o), Pedersen (σ_P), and Hall conductivity (σ_H) are the following [50]:

$$\sigma_o = \frac{N_e e^2}{m_e \nu_e} \tag{1}$$

where N_e, e, and m_e are the electron density, electric charge, and electron mass, respectively.

$$\sigma_P = \sigma_o \frac{(1+k)\nu_e^2}{(1+k)^2\nu_e^2 + \omega_e^2} \tag{2}$$

$$\sigma_H = \sigma_o \frac{\omega_e \nu_e}{(1+k)^2\nu_e^2 + \omega_e^2} \tag{3}$$

From Equations (1, 2, and 3), the values of κ and ν_e are expressed as follows:

$$k = \frac{\omega_e \omega_i}{\nu_e \nu_i} \tag{4}$$

and

$$\nu_e = \nu_{en} + \nu_{ei}; \quad \nu_i = \nu_{in} \tag{5}$$

where ω_e, ω_i, ν_{en}, ν_{ei}, and ν_{in} are the electron cyclotron frequency, ion cyclotron frequency, electron-neutral collision frequency, electron-ion collision frequency, and ion-neutral collision frequency, respectively. This study analyzes the daily height profile variations of ionospheric conductivity in the Ethiopian ionosphere during a very low solar activity in 24 hours of a day with selected four hours at midnight (00.00 UT), morning (09.00 UT), midday (12.00 UT), and early nighttime (18.00 UT) in Addis Ababa with geographic latitude 9° N and longitude 39° E. The monthly variations of ionospheric conductivity of parallel, Pedersen, and Hall conductivity are presented all months, with the highest ionospheric variability considered to occur after noontime, which is 14.00 UT hour. The height profiles of the study are between 80 km and 500 km with a 10 km interval, which is considered to be where more ionospheric variability takes place. Both the height and time variability of the ionospheric conductivity are considered in the analysis of the study.

III. Result and Discussion

Diurnal Variations of Ionospheric Conductivity

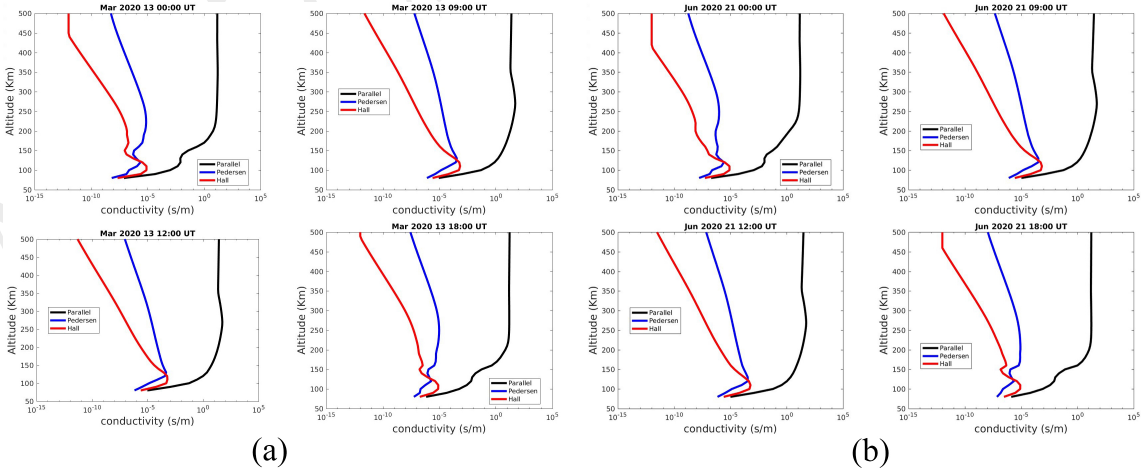

Figure 1. Diurnal variability of the ionospheric conductance of the parallel, Pedersen, and Hall conductivitie at the hours of 00:00, 09:00, 12:00, and 18:00 UT in Addis Ababa, (a) March 13, 2020 and (b) June 21, 2020.

The diurnal variability of ionospheric conductivity is the variation in conductance from day to night over a 24-hour period. As shown in Fig. 1(a), parallel conductivity rises noticeably from a height of 80

km to 350 km at 00.00 UT. On 00.00 UT, the parallel conductivity reached a peak of 15.85 S/m at 350 km and then decreased slightly up to 500 km. The Pedersen conductivity at 00.00 UT shows some variability, reaches its peak value at 220 km, and then decreases noticeably up to 500 km. At 00.00 UT, the Hall conductivity increased from 80 km to 110 km, reaching its maximum value 7.907×10^{-6} S/m at 110 km. After 110 km, the Hall conductivity begins to decrease noticeably, with some variability values reaching 500 km. At 09:00 UT on March 13, 2020, the parallel conductivity increased from 80 km to 270 km, attained its maximum value of 52.23 S/m at 270 km height, and decreased slightly from 270 km to 500 km. The Pedersen conductivity slightly increases from 80 km to 130 km, and attains a peak (3.5×10^{-6} S/m) at 130 km. The Hall conductivity slightly increases from 80 km to 110 km, slightly decreases with increasing height up to 500 km, and attains a peak (6.9×10^{-6} S/m) at 110 km. At 12:00 UT, parallel conductivity increases from 80 km to 270 km, and decreases slightly from 270 km to 500 km, reaches its maximum value of 53.52 S/m at 270 km. The Hall conductivity sightly increases from 80 km to 110 km and decreases with increases in height up to 500 km, attaining its peak value (5.9×10^{-6} S/m) at 110 km.

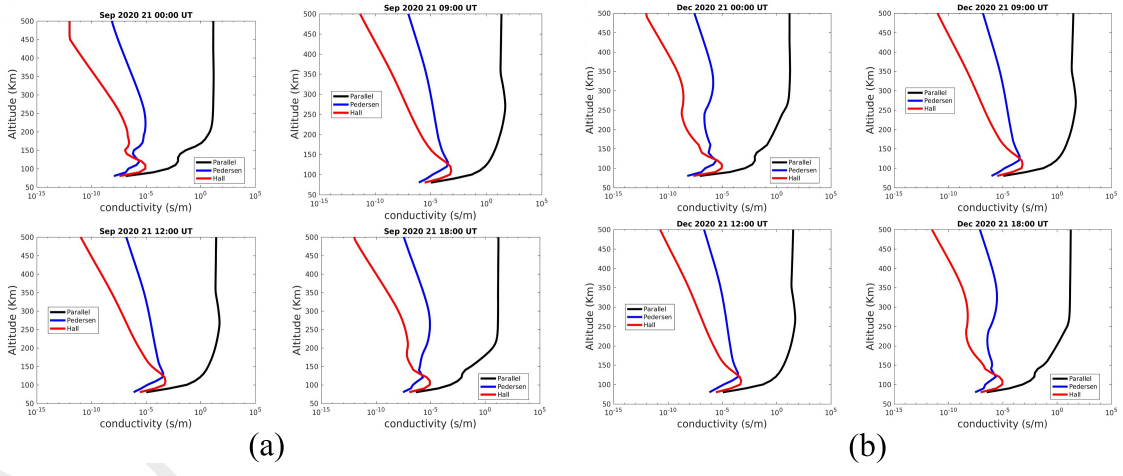

Figure 2. Diurnal variability of the ionospheric conductance of the parallel, Pedersen, and Hall conductivities at midnight (00:00 UT), morning (09:00 UT), midday (12:00 UT), and early nighttime (18:00 UT) in Addis Ababa, (a) September 21, 2020 and (b) December 21, 2020.

At early nighttime (18.00 UT), the parallel conductivity has a maximum peak value of 16.51 S/m at a higher height profile of 500 km than the other hours. The Pedersen and Hall conductivity have peak values of 9.6×10^{-6} S/m and 8.3×10^{-6} S/m at height profiles of 250 and 110 km, respectively. Fig. 1(b) indicates that the diurnal variability of the conductance on June 21, 2020, the parallel conductivity has peak values of 15.7 S/m, 52.51 S/m, 52.29 S/m, and 17.13 S/m at 00:00, 09:00, 12:00, and 18:00 UT with height profiles of 350, 270, 270, and 260 km, respectively. The Pedersen conductivity increases starting from 80 km to 120 km, with some fluctuations at 00.00 UT. The maximum values of the Pedersen

conductivity are attained at 210 km with 8.6×10^{-6} S/m.

From Fig. 2(a), the parallel conductivity at 18:00 UT has maximum values at 500 km (2.3×10^{-4} S/m). The Pedersen conductivity also attained a maximum value at 260 km (8.8×10^{-6} S/m) at 18:00 UT, respectively. At 00:00, 09:00, 12:00, and 18:00 UT, the Hall conductivity has peak values at 110 km (6.8×10^{-6} S/m). The hourly variability of December 21, 2020, is presented for midnight (00:00 UT), morning (09:00 UT), midday (12:00 UT), and early night (18:00 UT) (Fig. 2(b)). The maximum values of parallel conductivity are attained at heights of 500 km (2.3×10^{-4}).

Monthly Variations of Ionospheric Conductivity

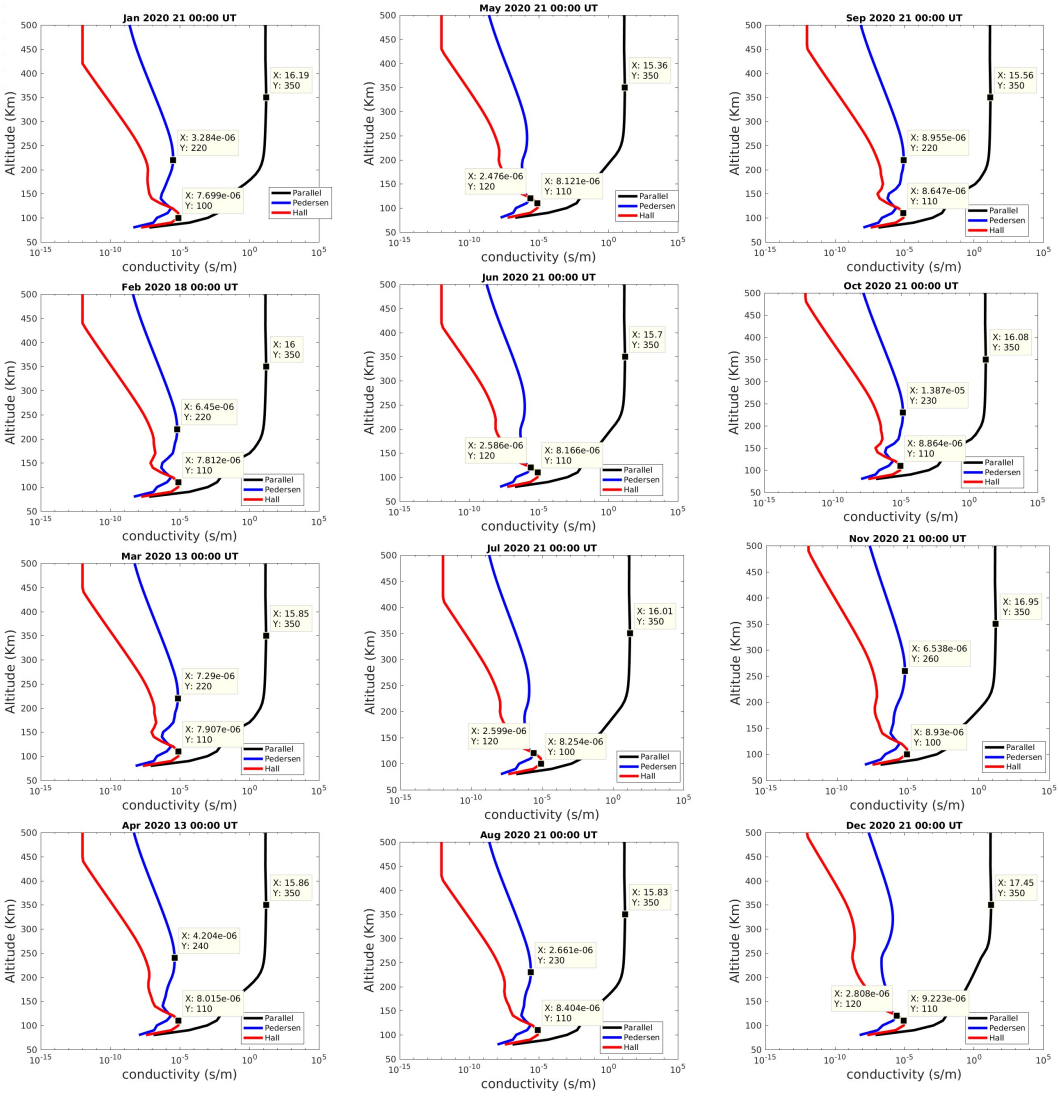

Figure 3. Monthly variability of the parallel, Pedersen, and Hall conductivity in the Addis Ababa ionosphere at 00.00 UT hour in the year 2020.

The monthly variability of the ionospheric conductivities is presented for all months of the year 2020 (Fig. 3 and Fig. 4). More ionospheric conductivity variations take place at 14:00 and 00:00 UT. The parallel conductivity varies between 15 and 18 S/m peak values with a constant height of 350 km, and the Pedersen conductivity maximum value location shows some height profile variations(Fig. 3). The height affects hall conductivity, with maximum values of 100 and 110 km(2.12×10^{-6} S/m). At midnight (00:00 UT) and early nighttime (18:00 UT), the ionospheric conductivity shows more fluctuation than in the morning (09:00 UT) and midday (12:00 UT), mostly in the D and E regions. This is due to disturbances associated with field-aligned currents [51] and the E and F regions of the solar wind systems [52]. The complexity in chemical and photochemical processes may be characterized by low density and high ionization collision frequencies of electrons with ions and neutral particles [53].

The nighttime ionospheric conductivity is disturbed more than the daytime, but the daytime conductivity value is greater in magnitude than the nighttime (Fig. 1 and Fig. 2). The height peak value of the nighttime is higher than the height peak of the daytime. Plasma transport is an important factor in determining the conductivity at high altitudes due to the coupling between the winds, plasma motion, and plasma density. This is more common in the parallel conductivity than the other two conductivities (Fig. 1 and Fig. 2). The parallel conductivity hourly variability of the December 21, 2020 peak value in height (350, 270, 270, and 500) km is 17.45, 53.73, 52.43, and 18.1 S/m, respectively. This is why in F-region ionospheric conductivity, the plasma distribution is largely determined by the plasma motion [54–56] and the wind is affected by plasma collisions and the ion drag forces producing the plasma motion, as well as the plasma motion itself, which are coupled to the neutrals. The Pedersen and Hall conductivities, on the other hand, are largely determined by the most significant currents that flow perpendicular to the magnetic field as well as altitude and local time change.

The monthly variations of ionospheric conductivity (parallel, Pedersen, and Hall) are presented in the daytime at 14:00 UT. In Fig. 3 and Fig. 4, the peak values of the parallel, Pedersen, and Hall conductivities are indicated with their corresponding height profile locations. From Fig. 4, June with 3.5×10^{-4} S/m and November with 3.5×10^{-4} S/m have the highest and lowest peak values of the ionospheric parallel conductivity, and for Hall conductivity, July has the greatest peak value (3.8×10^{-4} S/m) among all months. The three types of ionospheric conductivities increase steeply to reach their peak values. Each month, no significant variation in ionospheric conductivities is observed; this is due to less disturbance of the daytime solar activity during the very low solar activity phase.

Generally, the electron and ion Pedersen layers had different peak locations in the horizontal planes; these altitude differences in the horizontal distribution of the Pedersen conductivity affect the closed state of field-aligned currents associated with the D regions. The daily fluctuations of the magnetic field of the Earth are caused primarily by currents flowing in the ionospheric E-region but also in the lower F-region [57–60], which is generated by a combination of the neutral-wind dynamo moving plasma across

geomagnetic field lines and high latitude field-aligned currents that result in ionospheric conductivities.

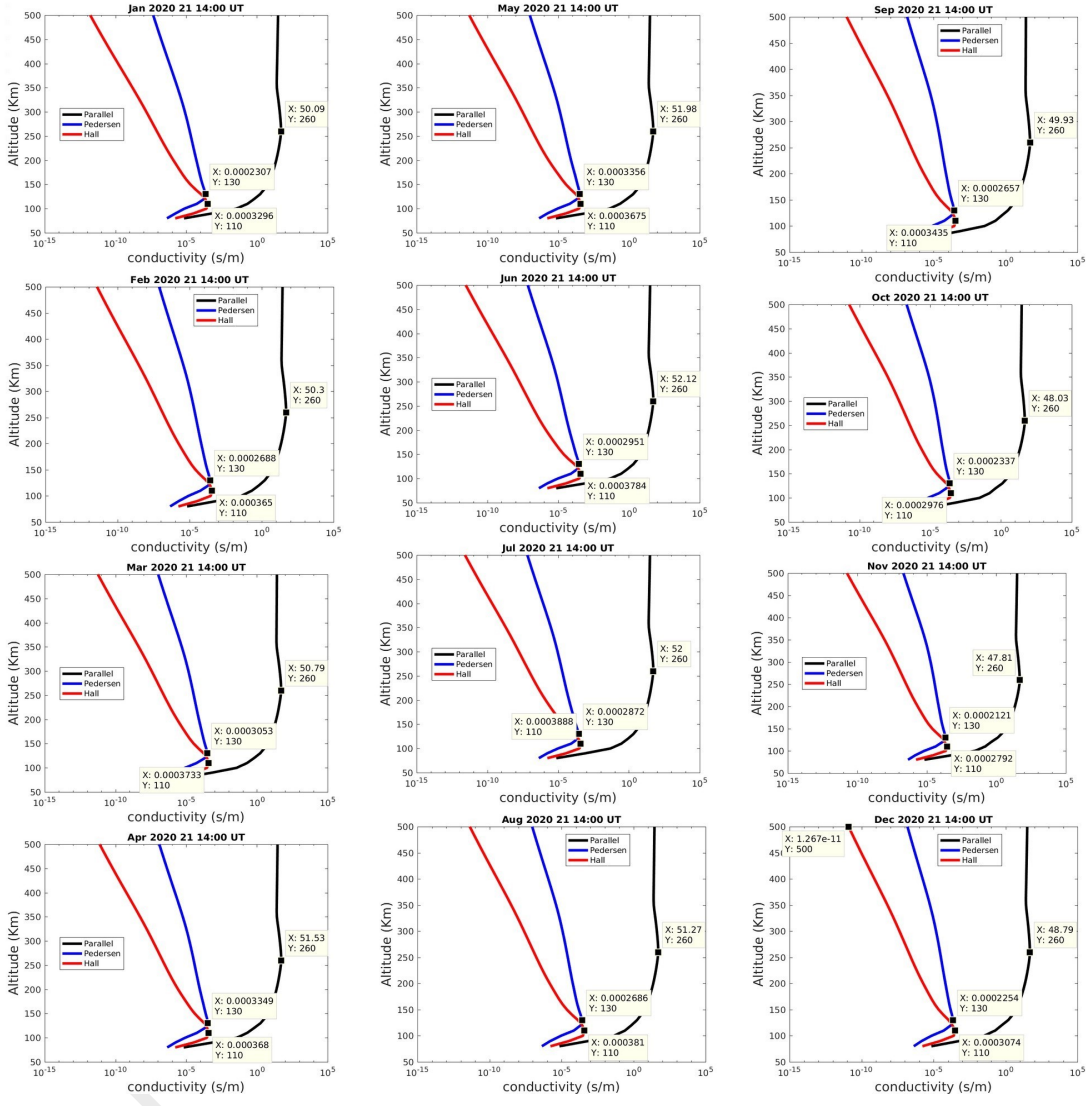

Figure 4. Monthly variability of conductivity in Addis Ababa in 2020.at 14.00 UT on the day of 21 in each month of the year 2020.

IV. Conclusion

In this work, we examined the height profiles of ionospheric conductivity for hourly and monthly variations in Addis Ababa, Ethiopia, during a very low solar activity phase in 2020. It is proposed that fluctuations in nightside ionospheric conductivity could be the root cause of the monthly and daily variation. Ionospheric conductivity plays a significant role in particle acceleration and the formation of geomagnetic disturbances. Additionally, we demonstrate how auroral and geomagnetic activity development is facilitated by low ionospheric conductivity. The variation of the geomagnetic field in the earth's

core is caused by ionospheric current, and it is determined by the ratio of gyro-frequencies to collision frequencies with height profiles. The current flow is based on Ohm's law, and the geomagnetic field makes the electric conductivity isotropic to present the parallel, Pedersen, and Hall conductivities. The nighttime ionospheric conductivity shows more fluctuation than the daytime because of disturbances from associated field-aligned currents and solar wind systems. The monthly variations of ionospheric conductivity of parallel, Pedersen, and Hall conductivity in the daytime at 14.00 UT hour have no significant variability in each month; this is due to less solar activity disturbance during the daytime in the very low solar activity phase. The monthly daytime ionospheric conductivity variation is not much more disturbed in a period of low solar activity at Addis Ababa.

V. Acknowledgements

The authors acknowledge that the team at the IRI recognizes the need to develop and maintain the IRI ionospheric conductivity model at the World Data Center for Geomagnetism, Kyoto (http://wdc.kugi.kyoto-u.ac.jp/ionocond/sigcal/index.html).

References

[1] Menk F, Orr D, Clilverd M, Smith A, Waters C, Milling D, et al. Monitoring spatial and temporal variations in the dayside plasmasphere using geomagnetic field line resonances. Journal of Geophysical Research: Space Physics. 1999;104(A9):19955-69.

[2] Raeder J, Wang Y, Fuller-Rowell TJ. Geomagnetic storm simulation with a coupled magnetosphere-ionosphere-thermosphere model. GEOPHYSICAL MONOGRAPH-AMERICAN GEOPHYSICAL UNION. 2001;125:377-84.

[3] Tóth G, Sokolov IV, Gombosi TI, Chesney DR, Clauer CR, De Zeeuw DL, et al. Space Weather Modeling Framework: A new tool for the space science community. Journal of Geophysical Research: Space Physics. 2005;110(A12).

[4] Heelis R, Maute A. Challenges to understanding the Earth's ionosphere and thermosphere. Journal of Geophysical Research: Space Physics. 2020;125(7):e2019JA027497.

[5] Yamazaki Y, Maute A. Sq and EEJ—a review on the daily variation of the geomagnetic field caused by ionospheric dynamo currents. Space Science Reviews. 2017;206(1):299-405.

[6] Richmond A. Ionospheric wind dynamo theory: A review. Journal of geomagnetism and geoelectricity. 1979;31(3):287-310.

[7] Hardy DA, Gussenhoven M, Holeman E. A statistical model of auroral electron precipitation. Journal of Geophysical Research: Space Physics. 1985;90(A5):4229-48.

[8] Salem MA, Liu N, Rassoul HK. Modification of the lower ionospheric conductivity by thunderstorm electrostatic fields. Geophysical Research Letters. 2016;43(1):5-12.

[9] Nagai T, Shinohara I, Fujimoto M, Machida S, Nakamura R, Saito Y, et al. Structure of the Hall current system in the vicinity of the magnetic reconnection site. Journal of Geophysical Research: Space Physics. 2003;108(A10).

[10] Ridley A, Deng Y, Toth G. The global ionosphere–thermosphere model. Journal of Atmospheric and Solar-Terrestrial Physics. 2006;68(8):839-64.

[11] Jin H, Miyoshi Y, Fujiwara H, Shinagawa H, Terada K, Terada N, et al. Vertical connection from the tropospheric activities to the ionospheric longitudinal structure simulated by a new Earth's whole atmosphere-ionosphere coupled model. Journal of Geophysical Research: Space Physics. 2011;116(A1).

[12] Wang H, Fuller-Rowell T, Akmaev R, Hu M, Kleist D, Iredell M. First simulations with a whole atmosphere data assimilation and forecast system: The January 2009 major sudden stratospheric warming. Journal of Geophysical Research: Space Physics. 2011;116(A12).

[13] Wang H, Fuller-Rowell T, Akmaev R, Hu M, Kleist D, Iredell M. Correction to "First simulations with a whole atmosphere data assimilation and forecast system: The January 2009 major sudden stratospheric warming". J Geophys Res. 2012;117:A03326.

[14] Siscoe G, Maynard N. Distributed two-dimensional region 1 and region 2 currents: Model results and data comparisons. Journal of Geophysical Research: Space Physics. 1991;96(A12):21071-85.

[15] Siscoe G, Crooker N, Erickson G, Sonnerup B, Siebert K, Weimer D, et al. Global geometry of magnetospheric currents inferred from MHD simulations. GEOPHYSICAL MONOGRAPH-AMERICAN GEOPHYSICAL UNION. 2000;118:41-52.

[16] Schuster A. XV. The diurnal variation of terrestrial magnetism. Philosophical Transactions of the Royal Society of London(A). 1889;(180):467-518.

[17] Friis-Christensen E. High latitude ionospheric currents. In: Exploration of the Polar Upper Atmosphere: Proceedings of the NATO Advanced Study Institute held at Lillehammer, Norway, May 5–16, 1980. Springer; 1980. p. 315-28.

[18] Thayer J. Height-resolved Joule heating rates in the high-latitude E region and the influence of neutral winds. Journal of Geophysical Research: Space Physics. 1998;103(A1):471-87.

[19] Wiltberger M, Wang W, Burns A, Solomon S, Lyon J, Goodrich C. Initial results from the coupled magnetosphere ionosphere thermosphere model: Magnetospheric and ionospheric responses. Journal of atmospheric and solar-terrestrial physics. 2004;66(15-16):1411-23.

[20] Thayer J, Vickrey J, Heelis R, Gary J. Interpretation and modeling of the high-latitude electromagnetic energy flux. Journal of Geophysical Research: Space Physics. 1995;100(A10):19715-28.

[21] Strangeway RJ. The equivalence of Joule dissipation and frictional heating in the collisional iono-

sphere. Journal of Geophysical Research: Space Physics. 2012;117(A2).

[22] Sheng C, Deng Y, Lu Y, Yue X. Dependence of Pedersen conductance in the E and F regions and their ratio on the solar and geomagnetic activities. Space Weather. 2017;15(3):484-94.

[23] Singer SF, Maple E, Bowen Jr W. Evidence for ionosphere currents from rocket experiments near the geomagnetic equator. Journal of Geophysical Research. 1951;56(2):265-81.

[24] Cahill Jr LJ. Investigation of the equatorial electrojet by rocket magnetometer. Journal of Geophysical Research. 1959;64(5):489-503.

[25] Davis TN, Burrows K, Stolarik JD. A latitude survey of the equatorial electrojet with rocket-borne magnetometers. Journal of Geophysical research. 1967;72(7):1845-61.

[26] Maynard NC. Measurements of ionospheric currents off the coast of Peru. Journal of Geophysical Research. 1967;72(7):1863-75.

[27] Yabuzaki T, Ogawa T. Rocket measurement of Sq ionospheric currents over Kagoshima, Japan. Journal of Geophysical Research. 1974;79(13):1999-2001.

[28] Pfaff RF. The near-Earth plasma environment. Space science reviews. 2012;168:23-112.

[29] Brekke A, Doupnik JR, Banks P. Incoherent scatter measurements of E region conductivities and currents in the auroral zone. Journal of Geophysical Research. 1974;79(25):3773-90.

[30] Moen J, Brekke A. On the importance of ion composition to conductivities in the auroral ionosphere. Journal of Geophysical Research: Space Physics. 1990;95(A7):10687-93.

[31] Robinson R, Vondrak R, Miller K, Dabbs T, Hardy D. On calculating ionospheric conductances from the flux and energy of precipitating electrons. Journal of Geophysical Research: Space Physics. 1987;92(A3):2565-9.

[32] McGranaghan R, Knipp DJ, Matsuo T, Godinez H, Redmon RJ, Solomon SC, et al. Modes of high-latitude auroral conductance variability derived from DMSP energetic electron precipitation observations: Empirical orthogonal function analysis. Journal of Geophysical Research: Space Physics. 2015;120(12):11-013.

[33] McGranaghan R, Knipp DJ, Matsuo T, Cousins E. Optimal interpolation analysis of high-latitude ionospheric Hall and Pedersen conductivities: Application to assimilative ionospheric electrodynamics reconstruction. Journal of Geophysical Research: Space Physics. 2016;121(5):4898-923.

[34] Rasmussen C, Schunk RW, Wickwar VB. A photochemical equilibrium model for ionospheric conductivity. Journal of Geophysical Research: Space Physics. 1988;93(A9):9831-40.

[35] Robinson R, Vondrak R. Measurements of E region ionization and conductivity produced by solar illumination at high latitudes. Journal of Geophysical Research: Space Physics. 1984;89(A6):3951-6.

[36] Richmond A. Modeling the ionosphere wind dynamo: A review. pure and applied geophysics. 1989;131:413-35.

[37] Richmond A, Maute A. Ionospheric electrodynamics modeling. Modeling the ionosphere–

thermosphere system. 2014:57-71.

[38] Ebihara Y, Fok MC, Wolf R, Immel T, Moore T. Influence of ionosphere conductivity on the ring current. Journal of Geophysical Research: Space Physics. 2004;109(A8).

[39] Yue X, Schreiner WS, Kuo YH, Wu Q, Deng Y, Wang W. GNSS radio occultation (RO) derived electron density quality in high latitude and polar region: NCAR-TIEGCM simulation and real data evaluation. Journal of Atmospheric and Solar-Terrestrial Physics. 2013;98:39-49.

[40] Sheng C, Deng Y, Yue X, Huang Y. Height-integrated Pedersen conductivity in both E and F regions from COSMIC observations. Journal of Atmospheric and Solar-Terrestrial Physics. 2014;115:79-86.

[41] Qian L, Solomon SC. Thermospheric density: An overview of temporal and spatial variations. Space science reviews. 2012;168:147-73.

[42] Emmert JT. Thermospheric mass density: A review. Advances in Space Research. 2015;56(5):773-824.

[43] Prölss GW. Density perturbations in the upper atmosphere caused by the dissipation of solar wind energy. Surveys in Geophysics. 2011;32:101-95.

[44] Liu H, Thayer J, Zhang Y, Lee WK. The non–storm time corrugated upper thermosphere: What is beyond MSIS? Space Weather. 2017;15(6):746-60.

[45] Fuller-Rowell T, Evans D. Height-integrated Pedersen and Hall conductivity patterns inferred from the TIROS-NOAA satellite data. Journal of Geophysical Research: Space Physics. 1987;92(A7):7606-18.

[46] Kirkwood S, Opgenoorth H, Murphree J. Ionospheric conductivities, electric fields and currents associated with auroral substorms measured by the EISCAT radar. Planetary and Space Science. 1988;36(12):1359-80.

[47] Aksnes A, Stadsnes J, Bjordal J, Østgaard N, Vondrak R, Detrick D, et al. Instantaneous ionospheric global conductance maps during an isolated substorm. In: Annales Geophysicae. vol. 20. Copernicus Publications Göttingen, Germany; 2002. p. 1181-91.

[48] Giannattasio F, De Michelis P, Pignalberi A, Coco I, Consolini G, Pezzopane M, et al. Parallel electrical conductivity in the topside ionosphere derived from swarm measurements. Journal of Geophysical Research: Space Physics. 2021;126(2):e2020JA028452.

[49] Maeda Ki. Conductivity and drifts in the ionosphere. Journal of Atmospheric and Terrestrial Physics. 1977;39(9-10):1041-53.

[50] Wiltberger M, Merkin V, Zhang B, Toffoletto F, Oppenheim M, Wang W, et al. Effects of electrojet turbulence on a magnetosphere-ionosphere simulation of a geomagnetic storm. Journal of Geophysical Research: Space Physics. 2017;122(5):5008-27.

[51] Richmond A. The ionospheric wind dynamo: Effects of its coupling with different atmospheric regions. The Upper Mesosphere and Lower Thermosphere: A Review of Experiment and Theory,

Geophys Monogr Ser. 1995;87:49-65.

[52] Coley W, Heelis R, Spencer N. Comparison of low-latitude ion and neutral zonal drifts using DE 2 data. Journal of Geophysical Research: Space Physics. 1994;99(A1):341-8.

[53] Endeshaw L. Testing and validating IRI-2016 model over Ethiopian ionosphere. Astrophysics and Space Science. 2020;365(3):49.

[54] Pfaff Jr RF, Acuña MH, Marionni PA, Trivedi NB. DC polarization electric field, current density, and plasma density measurements in the daytime equatorial electrojet. Geophysical Research Letters. 1997;24(13):1667-70.

[55] Richmond A, Thayer J. Ionospheric electrodynamics: A tutorial. Magnetospheric current systems. 2000;118:131-46.

[56] Sultan P. Linear theory and modeling of the Rayleigh-Taylor instability leading to the occurrence of equatorial spread F. Journal of Geophysical Research: Space Physics. 1996;101(A12):26875-91.

[57] Li Z, Lei J, Zhang B. Three-Dimensional Simulation of Equatorial Spread F: Effects of Field-Aligned Plasma Flow and Ionospheric Conductivity. Journal of Geophysical Research: Space Physics. 2023;128(3):e2022JA031070.

[58] Smotrova EE, Mager PN, Mikhailova OS, Klimushkin DY. Diagnostics of the ionospheric conductivity based on spacecraft observations of the magnetospheric ULF waves. Journal of Geophysical Research: Space Physics. 2023;128(7):e2023JA031441.

[59] Fukizawa M, Tanaka Y, Ogawa Y, Hosokawa K, Raita T. Three-dimensional ionospheric conductivity associated with pulsating auroral patches: reconstruction from ground-based optical observations. Annales Geophysicae Discussions. 2023;2023:1-25.

[60] Endeshaw L, Seyoum A. Performance evaluation of IRI-Plas 2017 model with ionosonde data measurements of ionospheric parameters. Heliyon. 2023;9(11).